Int. J. Electrochem. Sci., 7 **(2012)** 11966 - 11977

International Journal of
ELECTROCHEMICAL
SCIENCE
www.electrochemsci.org

Microstructures and Electrochemical Properties of $LaNi_{3.55}Co_{0.2-x}Mn_{0.35}Al_{0.15}Cu_{0.75}(V_{0.81}Fe_{0.19})_x$ Hydrogen Storage Alloys

Baozhong Liu[1,*], *Xianyun Peng*[1], *Yanping Fan*[1], *Liqiang Ji*[2], *Baoqing Zhang*[1], *Zhi Zhang*[1]

[1] School of Materials Science and Engineering, Henan Polytechnic University, Jiaozuo 454000, China
[2] Inner Mongolia Rare Earth Ovonic Metal Hydride Co. Ltd., Baotou 014030, China
[*]E-mail: b_z_liu@163.com

Received: 27 September 2012 / *Accepted:* 19 October 2012 / *Published:* 1 December 2012

Microstructures and electrochemical characteristics of $LaNi_{3.55}Co_{0.2-x}Mn_{0.35}Al_{0.15}Cu_{0.75}(V_{0.81}Fe_{0.19})_x$ hydrogen storage alloys were investigated. X-ray diffraction and Backscatter electron results indicate that $LaNi_{3.55}Co_{0.2}Mn_{0.35}Al_{0.15}Cu_{0.75}$ alloy is single $LaNi_5$ phase, and the alloys containing $V_{0.81}Fe_{0.19}$ consist of $LaNi_5$ phase, Ni-rich second phase and La-rich segregation, and the abundant of secondary phase increases with increasing x value. The activation property of the alloy electrodes is improved by increasing $V_{0.81}Fe_{0.19}$ content. Maximum discharge capacity of the alloy electrodes first increases from 325.9 mAh/g (x = 0) to 330.3 mAh/g (x = 0.05), and then decreases to 301.3 mAh/g (x = 0.20). HRD_{1200} first increases from 43.3% (x = 0) to 58.5% (x = 0.05), and then decreases to 47.4% (x = 0.20). Cycling stability decreases with increasing x from 0 to 0.20.The adequate substitution of Co by VFe can improve the electrochemical performances and reduce the raw cost of alloy electrode.

Keywords: Hydrogen storage alloy; VFe alloy; Phase structure; Electrochemical property; Ni/MH batteries

1. INTRODUCTION

AB_5-type alloys have attracted much attention due to their widespread applications in rechargeable nickel/metal hydride (Ni/MH) batteries [1]. In order to broaden application field of Ni/MH batteries and enhance their competition abilities, a realistic approach is to reduce the cost of AB_5-type alloy [2]. The cost of cobalt is the highest among raw material of AB_5-type alloy, and many attempts have been made to decrease the cost of alloy by substituting Co with foreign metals, such as, Fe, Cu, Si etc, whose raw cost was much cheaper compared with Co [3-5]. The Co-less alloy with high Cu content was developed and exhibits excellent electrochemical properties [6]. However, the

performance-price ratio of the alloy electrode is still unsatisfactory. Consequently it is necessary to improve the electrochemical properties with reducing the raw cost of AB_5-type alloy.

Iron, which is less costly, is a 3d transition metal like cobalt, and substitute cobalt in AB_5 alloys without enough electronic perturbation [7,8]. It is believed that Fe is one of the best candidates for cobalt substitution [9-10]. However, iron addition is detrimental to charge-transfer reaction on the surface and hydrogen diffusion from the alloy bulk to the surface due to the iron oxidation on the alloy surface, and thus inevitably decreases the discharge capacity and high-rate dischargeability of alloy electrode. It is believed that the introduction of V into AB_5-type alloy can effectively contribute to the activation, discharge capacity and kinetic properties [11-13]. Therefore, it can be expected that the overall electrochemical properties should be improved by the substitution of Fe and V for Co in the alloy. However, the pure V is very expensive and unpractical to be used in the Co-less alloy. Fortunately, the cost of commercial $V_{0.81}Fe_{0.19}$ alloy is obviously lower than that of pure V and Co. Consequently, it is feasible and promising to substitute Ni by $V_{0.81}Fe_{0.19}$ in Co-less AB_5-type alloy.

In this work, on the basis of the merits of $V_{0.81}Fe_{0.19}$ and the belief that the Fe and V addition may result in some noticeable modification of the alloys, microstructures and electrochemical hydrogen storage properties of $LaNi_{3.55}Co_{0.2-x}Mn_{0.35}Al_{0.15}Cu_{0.75}(V_{0.81}Fe_{0.19})_x$ (x = 0-0.20) alloys have been investigated systematically.

2. EXPERIMENTAL PROCEDURES

$LaNi_{3.55}Co_{0.2-x}Mn_{0.35}Al_{0.15}Cu_{0.75}(V_{0.81}Fe_{0.19})_x$ (x = 0-0.20) alloys were synthesized by induction melting of the metal elements (La, Ni, Co, Mn, Al, Cu: 99.9% purity and commercial $V_{0.81}Fe_{0.19}$ alloy contained 81% V and the other were Fe and trace impurities.) under argon atmosphere and then were annealed at 1273 K for 10 h under argon atmosphere with the pressure of 0.08 MPa..

The phases of the alloy powders were determined by X-ray diffraction (XRD) using a Rigaku D/max 2500PC powder diffractometer with Cu Kα radiation. The phase structures of alloys were analyzed using Jade-5 software. Back Scatter Electron (BSE) images were obtained by using HITACHI-4800 scanning electron microscope.

All the alloy electrodes for test were prepared by cold pressing the mixture of 0.15 g alloy powders of 200-400 meshes and 0.75 g nickel carbonyl powders into a pellet of 10 mm in diameter under 15 MPa. Electrochemical measurements were performed at 298 K in a standard tri-electrode system, consisting of a working electrode (metal hydride), a counter electrode ($Ni(OH)_2$/NiOOH), and a reference electrode (Hg/HgO) with 6mol/L KOH solution as electrolyte. Each electrode was charged for 7 h at 60 mA/g and discharged to -0.6 V versus Hg/HgO at 60 mA/g at 298 K. After every charging/discharging, the rest time was 10 min. In evaluating the high-rate dischargeability, discharge capacity of the alloy electrodes at different discharge current density was measured. The high-rate dischargeability HRD (%) defined as $C_n \times 100/(C_n + C_{60})$, was determined by the ratio of the discharge capacity C_n (n = 60, 300, 600, 900 and 1200) to the total discharge capacity defined as the sum of C_n and C_{60}, which was additional capacity measured subsequently at 60 mA/g after C_n was measured.

The linear polarization curve and potential-step measurement were obtained by Advanced Potentiostat/Galvanostat (PARSTAT 2273), respectively. At 50% depth of discharge (DOD), the linear polarization curve was obtained by scanning the electrodes from - 5 to 5 mV (vs.open circuit potential). For potential-step measurement, the electrodes in fully charged state were discharged with potential steps of 0.5 V for 3600 s.

3. RESULTS AND DISCUSSION

3.1 Crystal structure

Fig. 1 presents XRD patterns of $LaNi_{3.55}Co_{0.2-x}Mn_{0.35}Al_{0.15}Cu_{0.75}(V_{0.81}Fe_{0.19})_x$ alloys. It can be seen that $LaNi_{3.55}Co_{0.2-x}Mn_{0.35}Al_{0.15}Cu_{0.75}(V_{0.81}Fe_{0.19})_x$ alloys have a single $LaNi_5$ phase with $CaCu_5$ structure. The alloys containing $V_{0.81}Fe_{0.19}$ consist of the matrix $CaCu_5$-type phase with a small amount of the second phases, and the amount of second phase increases with increasing x value.

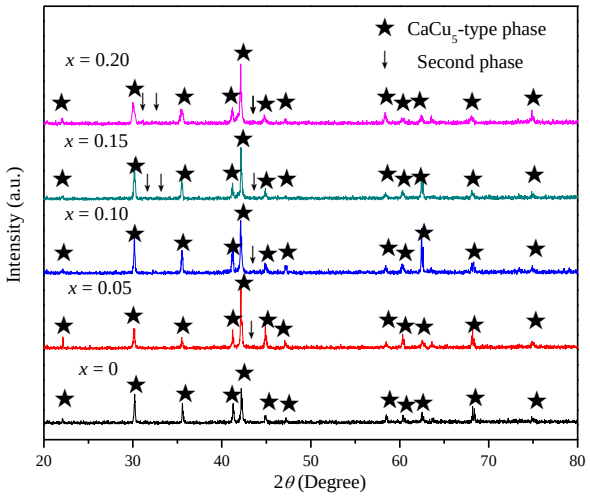

Figure 1. XRD patterns of $LaNi_{3.55}Co_{0.2-x}Mn_{0.35}Al_{0.15}Cu_{0.75}(V_{0.81}Fe_{0.19})_x$ alloys

Table 1. Lattice parameters of $LaNi_{3.55}Co_{0.2-x}Mn_{0.35}Al_{0.15}Cu_{0.75}(V_{0.81}Fe_{0.19})_x$ alloys

x	a (Å)	c (Å)	V (Å^3)
0	5.04819	4.03881	89.1339
0.05	5.05271	4.03428	89.1934
0.10	5.04583	4.05045	89.3072
0.15	5.05849	4.04133	89.5538
0.20	5.05788	4.04321	89.5739

The calculated lattices parameters of $LaNi_5$ phase in all alloys are listed in Table 1. It can be seen that *a* and *V* increase with the increase of *x* value. Fig. 2 is the BSE images of $LaNi_{3.55}Co_{0.2-x}Mn_{0.35}Al_{0.15}Cu_{0.75}(V_{0.81}Fe_{0.19})_x$ alloys. Through BSE analysis in Fig. 2(a), it is found that $LaNi_{3.55}Co_{0.2}Mn_{0.35}Al_{0.15}Cu_{0.75}$ alloy is single phase without continuous segregation. In Fig. 2(b), $LaNi_{3.55}Co_{0.2-x}Mn_{0.35}Al_{0.15}Cu_{0.75}(V_{0.81}Fe_{0.19})_{0.20}$ alloy consists of shallow black regions (A), white area (B) and little black bulk (C). According to EDS results listed in Table 2, the A, B and C correspond to $LaNi_5$ phase, Ni-rich second phase and La-rich segregation, respectively. The result is consistent with the literatures [11,12].

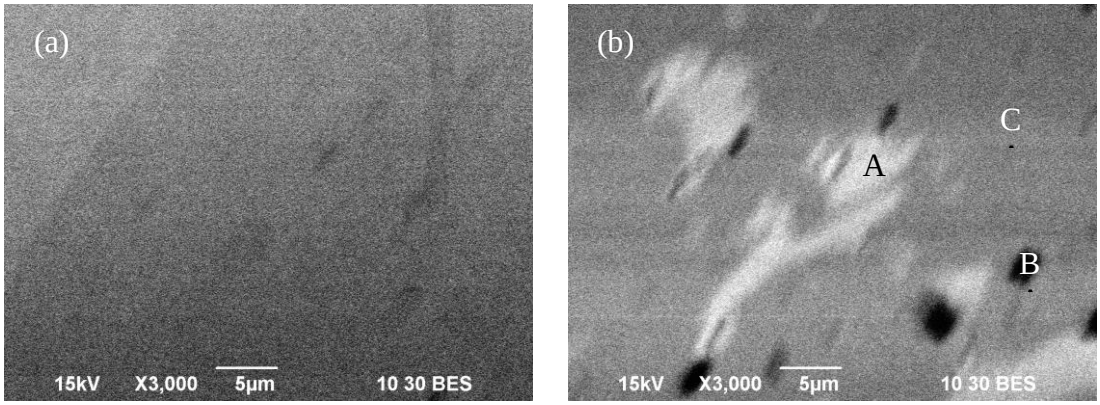

Figure 2. BSE images of $LaNi_{3.55}Co_{0.2-x}Mn_{0.35}Al_{0.15}Cu_{0.75}(V_{0.81}Fe_{0.19})_x$ alloys (a) $x = 0$ (b) $x = 0.20$

Table 2. EDS results of $LaNi_{3.55}Co_{0.2-x}Mn_{0.35}Al_{0.15}Cu_{0.75}(V_{0.81}Fe_{0.19})_x$ alloys

	A		B		C	
	mass%	at.%	mass%	at.%	mass%	at.%
La	37.70	19.45	45.83	25.83	18.38	8.35
Ni	42.40	51.77	33.67	44.74	53.02	56.99
Cu	9.04	10.19	9.13	11.20	7.15	7.10
Mn	5.94	7.75	4.95	7.03	5.67	6.51
Fe	3.54	4.54	2.56	3.57	1.81	2.04
Al	2.37	6.29	1.34	3.87	1.56	3.65
V			2.52	3.86	12.41	15.37

3.2 Activation capability and discharge capability

The number of cycles (N_a) needed to activate the electrodes and maximum discharge capacity (C_{max}) of $LaNi_{3.55}Co_{0.2-x}Mn_{0.35}Al_{0.15}Cu_{0.75}(V_{0.81}Fe_{0.19})_x$ alloy electrodes are given in Table 3. It was noted that N_a of alloy electrodes decreases with increasing *x* value, indicating that the activation property of the alloy electrodes increases with increasing $V_{0.81}Fe_{0.19}$ content. Soe et al. [11] pointed out

that the dissolution of V in the AB_5-type alloys makes the electrode surface change to microporous, which is very helpful to hydrogen penetration, and then improves the activation property. The increase in V content contributes to the improvement of activation property of alloy electrodes with increasing *x* value. Moreover, Shu et al. [14] and Zhang et al. [15] pointed out that the phase interface or grain boundary contributes to the activation of alloy electrode because the interface or boundary was a buffer area of the releasing of the lattice stress and strain energy. According to the XRD and BSE results, the phase interface increases with increasing *x* values, which is beneficial to the activation property. However, it is believed that the metalic Co in the alloy surface acts as an electrocatalyst for the rapid activation [16-18]. Co content on the surface of the alloy electrode decreases with increasing *x* value, which is detrimental to the activation properties. Consequently the advantageous factor is prominent for the improvement of the activation property of $LaNi_{3.55}Co_{0.2-x}Mn_{0.35}Al_{0.15}Cu_{0.75}(V_{0.81}Fe_{0.19})_x$ alloy electrodes. The C_{max} of the alloy electrodes first increases from 325.9 mAh/g (x = 0) to 330.3 mAh/g (x = 0.05), and then decreases to 301.3 mAh/g (x = 0.20). In general, the maximum discharge capacity is related to the crystalline structure and electrochemical kinetics. The addition of V in the AB_5 alloy contributed to the increase of discharge capacity [11]. The increase of V with increasing *x* value is beneficial to the maximum discharge capacity. Moreover, Brateng et al. [19] pointed out that the increase in cell volume contributes to the discharge capacity of AB_5 alloys. From the analysis of the calculated lattice parameters of the alloys, the *V* of $CaCu_5$-type increases with increasing *x* value, which is favorable to the discharge capacity. Unfortunately, Co contributes to the charge-transfer reaction at the electrode/electrolyte interface due to excellent electrocatalytic activity and makes the hydrogen diffusion through the surface more easily due to good electrical conductivity [20].

Table 3. Electrochemical characteristics of $LaNi_{3.55}Co_{0.2-x}Mn_{0.35}Al_{0.15}Cu_{0.75}(V_{0.81}Fe_{0.19})_x$ alloy electrodes

x	C_{max} (mAh/g)	HRD_{1200} [a] (%)	N_a [b]	S_{100}(%)
0	325.9	43.3	5	85.7
0.05	330.3	58.5	4	84.3
0.10	319.6	54.1	3	83.0
0.15	311.5	49.7	2	81.1
0.20	301.3	47.4	2	78.8

[a] The high-rate dischargeability at the discharge current density of 1200 mA g^{-1}.

[b] The number of cycles needed to activate the electrode.

As *x* increases, the increase in Fe content and the decrease of Co content degrade the charge-transfer reaction on the alloy surface and lead to a decrease of the discharge capacity.

3.3 High-rate dischargeability and electrochemical kinetics

As an important kinetics property of the hydride electrode in battery, it is very important to minimize the decrease in discharge capacity even at the high discharge current density [21]. Fig. 3

shows the relationship between the high-rate dischargeability (HRD) and the discharge current density of $LaNi_{3.55}Co_{0.2-x}Mn_{0.35}Al_{0.15}Cu_{0.75}(V_{0.81}Fe_{0.19})_x$ alloy electrodes. The HRD of the alloy electrodes first increases with increasing x from 0 to 0.05, and then decreases when x increases to 0.20. The HRD at the discharge current density of 1200 mA/g (HRD_{1200}) is listed in Table 3. It can be seen that HRD_{1200} first increases from 43.3% (x = 0) to 58.5% (x = 0.05), and then decreases to 47.4% (x = 0.20).

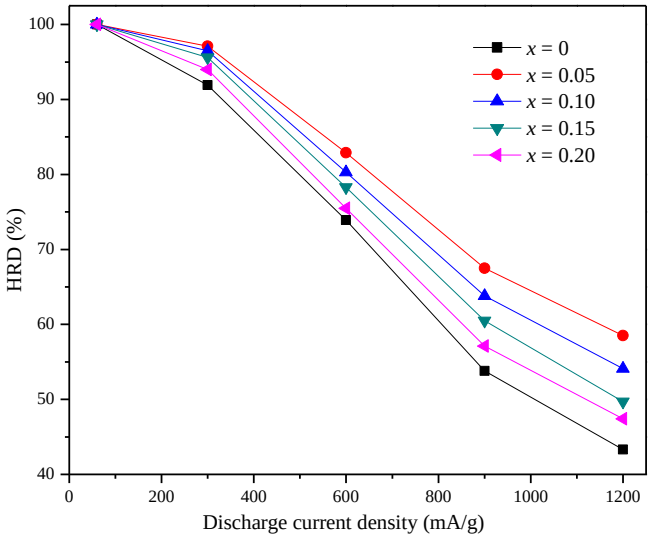

Figure 3. High-rate dischargeability of $LaNi_{3.55}Co_{0.2-x}Mn_{0.35}Al_{0.15}Cu_{0.75}(V_{0.81}Fe_{0.19})_x$ alloy electrodes

It is well known that the HRD of the metal-hydride electrodes is dominated by the charge-transfer reaction at the electrode/electrolyte interface and the hydrogen diffusion rate within the bulky alloy electrode, which are reflected in the value of surface exchange current density (I_0), being a measure of the catalytic activity of an alloy, as well as in the hydrogen diffusion coefficient (D), which characterizes the mass transport properties of an alloy electrode [22].

Exchange current density I_0 is the rate of hydriding/dehydriding at the equilibrium state and can be used to evaluate electrocatalytic activity for charge-transfer reaction on the surface of alloy electrodes. It can be determined from linear micropolarization curve. Fig. 4 shows the linear polarization curves of $LaNi_{3.55}Co_{0.2-x}Mn_{0.35}Al_{0.15}Cu_{0.75}(V_{0.81}Fe_{0.19})_x$ alloy electrodes at 50% DOD and 298 K. The polarization resistances R_p is calculated through estimating the slopes of linear polarization curves, and listed in Table 4. The R_p values of the alloy electrodes first decreases from 213.1 (x = 0) to 150.0 mΩ g (x = 0.05), and then increases to 203.0 mΩ g (x = 0.20) with increasing x value. The I_0 value can be calculated according to the following formula [23].

$$I_0 = \frac{RT}{FR_p} \qquad (1)$$

where R, T, F, R_p are the gas constant, absolute temperature, Faraday constant and the polarization resistance, respectively. The I_0 values are calculated by Eq. (1) listed in Table 4.

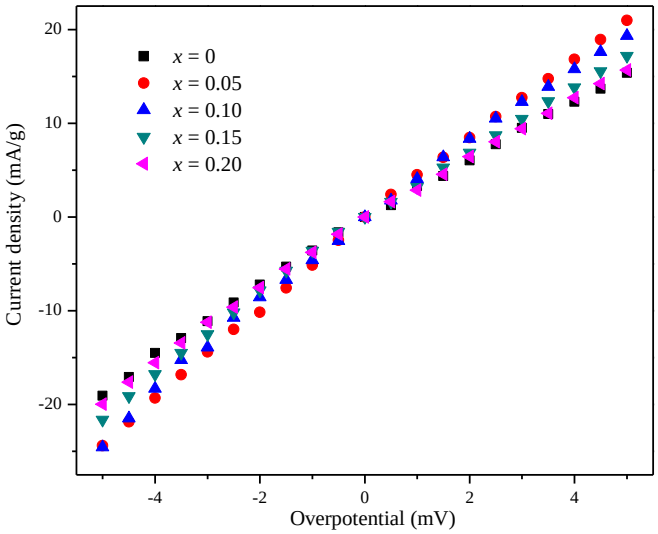

Figure 4. Linear polarization curves of of $LaNi_{3.55}Co_{0.2-x}Mn_{0.35}Al_{0.15}Cu_{0.75}(V_{0.81}Fe_{0.19})_x$ alloy electrodes at 50% DOD

Table 4. Electrochemical kinetic parameters of $LaNi_{3.55}Co_{0.2-x}Mn_{0.35}Al_{0.15}Cu_{0.75}(V_{0.81}Fe_{0.19})_x$ alloy electrodes

x	R_p (mΩ g)	I_0 (mA/g)	D ($\times 10^{-10}$ cm^2/s)
0	213.1	120.5	1.01
0.05	150.0	171.2	1.36
0.10	161.1	159.4	1.31
0.15	180.6	142.2	1.20
0.20	203.0	126.5	1.07

It is clear that the I_0 first increases from 120.5 mA/g (x = 0) to 171.2 mA/g (x = 0.05), and then decreases to 126.5 mA/g (x = 0.20). It is well known that rich-Ni phase exhibits excellent electrochemical catalytic activity due to high Ni content. According to the XRD and BSE results, the rich-Ni second phase increases with increasing x value, which is beneficial to the electrocatalytic activity of the surface of alloy electrode and improves the charge-transfer reaction. However, the increase of Fe and decrease of Co will cause the increase of surface oxide film and then degrade the charge-transfer reaction on the alloy surface. Therefore, it is reasonable to assume that, when $x \leq 0.05$, the favorable effect is chiefly responsible for the increase of the exchange current density for alloy electrodes. However, when x > 0.05, the decrease of the exchange current density for alloy electrodes is mainly ascribed to the disadvantageous factors. In present study, the critical content of $V_{0.81}Fe_{0.19}$ is x = 0.05.

The diffusion coefficient of hydrogen in the alloy electrodes is determined with the potential-step method. Fig. 5 shows the semi-logarithmic plots of the anodic current vs. the time response of $LaNi_{3.55}Co_{0.2-x}Mn_{0.35}Al_{0.15}Cu_{0.75}(V_{0.81}Fe_{0.19})_x$ alloy electrodes. It can be seen that the current-time responses can be divided into two time domains [24], in the first time region, the oxidation current of

hydrogen rapidly declines due to the rapid consumption of hydrogen on the surface. However, in the second time region followed, the current declines more slowly and drops linearly with time. Since hydrogen is supplied from the bulk of the alloy at a rate proportional to the concentration gradient of hydrogen, hence the electrode current is controlled by the diffusion of hydrogen in the second time region. Zheng et al. [24] reported that in a large anodic potential-step test, after a long discharge time, the diffusion current varies with time according to the following equation:

$$\lg i = \lg\left(\frac{6FD}{da^2}(C_0 - C_s)\right) - \frac{\pi^2}{2.303}\frac{D}{a^2}t \qquad (2)$$

where i is anodic current density (A/g), D the hydrogen diffusion coefficient (cm^2/s), d the density of the alloy (g/cm^3), a the radius of the alloy particle, C_0 the initial hydrogen concentration in the bulk of the alloy (mol/cm^3), C_s the surface hydrogen concentration of the alloy (mol/cm^3) and t is the discharge time (s).

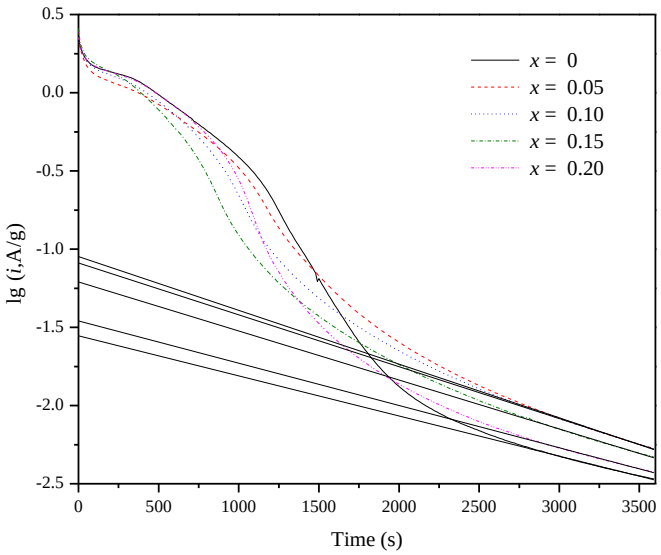

Figure 5. Semi-logarithmic plots of anodic current vs. time responses of $LaNi_{3.55}Co_{0.2-x}Mn_{0.35}Al_{0.15}Cu_{0.75}(V_{0.81}Fe_{0.19})_x$ alloy electrodes

Assuming that the alloy has a similar particle distribution with an average particle radius of 13 μm according to previous study[25], D was calculated and summarized in Table 4. The D of $LaNi_{3.55}Co_{0.2-x}Mn_{0.35}Al_{0.15}Cu_{0.75}(V_{0.81}Fe_{0.19})_x$ alloy electrodes first increases from 1.01×10^{-10} (x = 0) to 1.36×10^{-10} cm^2/s (x = 0.05), and then decreases to $1.07 \times 10^{-10} cm^2/s$ (x = 0.20). As mentioned above, the formation of the secondary phase increases the number of phase boundaries, which provides extra tunnels for the diffusion of hydrogen atoms and is buffer area of the releasing of the stress formed in the process of hydrogen absorbed. The increase of rich-Ni secondary phase causes the increase in the phase boundary, which can decrease the lattice distortion and strain energy formed in the process of hydrogen absorption. On the other hand, Iwakura et al. [26] have reported that the oxidation of Fe on

the alloy surface limited the hydrogen transfer from the bulk to the surface, which is detrimental to the hydrogen diffusion. As mentioned above, the increase of Fe content causes the increase of surface oxide film, which will degrade the hydrogen diffusion. Moreover, metalic Co on the alloy surface made the hydrogen diffuse from the bulk to the surface more easily due to the good electrocatalytic activity and electrical conductivity. The decrease of Co content is unfavorable to the hydrogen diffusion property. Therefore, it is certain that the diffusion coefficient has a maximum value with increasing *x* value.

Iwakura et al. [27] have reported that linear dependence of the high-rate dischargeability on exchange current density and activation energy of hydrogen diffusion indicated that the charge transfer and hydrogen diffusion are responsible for discharge efficiency. Fig. 6 shows the HRD_{1200} as a function of exchange current density and hydrogen diffusion coefficient for $LaNi_{3.55}Co_{0.2-x}Mn_{0.35}Al_{0.15}Cu_{0.75}(V_{0.81}Fe_{0.19})_x$ alloy electrodes. It is evident that the HRD_{1200} increases with the increase of I_0 and D, and shows a linear relationship with I_0 and D, respectively. This implies that both charge-transfer reaction at the electrode/electrolyte interface and the hydrogen diffusion of alloy electrodes should be responsible for the HRD at a discharge current density of 1200 mA/g.

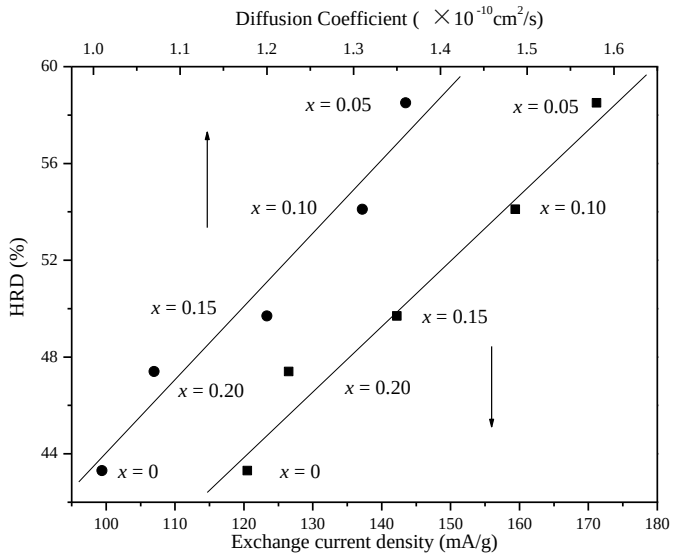

Figure 6. HRD at 1200 mA/g as a function of exchange current density for $LaNi_{3.55}Co_{0.2-x}Mn_{0.35}Al_{0.15}Cu_{0.75}(V_{0.81}Fe_{0.19})_x$ alloy electrodes

3.4 Cycling stability

The cycle stability is an extremely important factor for the service life of hydrogen storage alloys. The cycling capacity retention rate is expressed as $S_n(\%) = C_n/C_{max} \times 100$ (where C_n is the discharge capacity at the n^{th} cycle). The cycling capacity retention of $LaNi_{3.55}Co_{0.2-x}Mn_{0.35}Al_{0.15}Cu_{0.75}(V_{0.81}Fe_{0.19})_x$ alloy electrode as a function of cycle number is shown in Fig. 7. Cycling stability decreases with increasing *x* from 0 to 0.20. The cycling capacity retention rate after 100 charge/discharge cycles (S_{100}) is listed in Table 3.

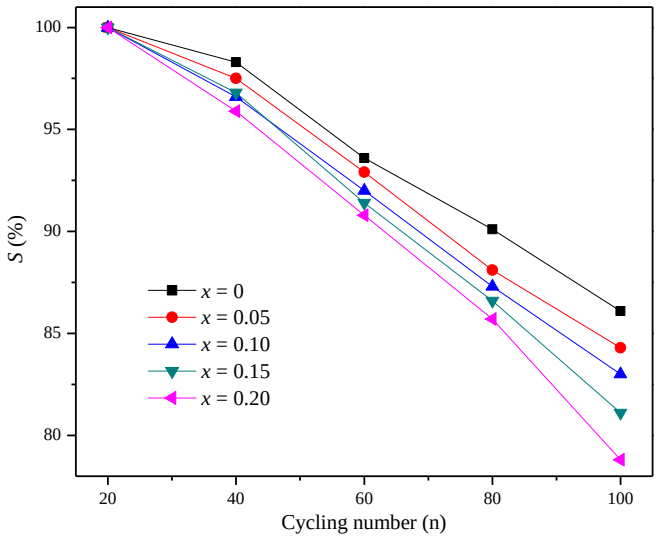

Figure 7. Cycling stability of $LaNi_{3.55}Co_{0.2-x}Mn_{0.35}Al_{0.15}Cu_{0.75}(V_{0.81}Fe_{0.19})_x$ alloy electrodes

It can be seen that S_{100} monotonically decreases from 85.7% (x = 0) to 78.8% (x = 0.20). The capacity decay of the hydrogen storage alloy electrode is mainly due to the pulverization and oxidation [28,29]. As mentioned above, the rich-Ni secondary phase increases the amount of phase boundary, which releases the stress formed in the process of hydrogen absorbing and then improves cycling stability. Moreover, Lin et al. [30] reported the increase of cell volume unit decreased the volume dilatation in the process of hydride formation, and therefore contributes to the charge-discharge life cycles. Unfortunately, it is well-known that Fe in the KOH solution more easily oxidized than Ni due to the lower surface energy of Fe. The increase in Fe and the decrease of Ni not only cause the deterioration of the corrosion resistance with increasing x value and then increase the loss of the alloy, but also degrade the electrochemical kinetics at the surface. Furthermore, it is reported that the V-dissolution caused shortening of cycle life [31].The increase in V with increasing x value is unfavorable for the cycling stability of the alloy electrodes. Consequently, the disadvantageous factor is prominent for the degradation of the cycling stability of $LaNi_{3.55}Co_{0.2-x}Mn_{0.35}Al_{0.15}Cu_{0.75}(V_{0.81}Fe_{0.19})_x$ alloy electrodes.

4. CONCLUSIONS

Microstructures and electrochemical characteristics of $LaNi_{3.55}Co_{0.2-x}Mn_{0.35}Al_{0.15}Cu_{0.75}(V_{0.81}Fe_{0.19})_x$ hydrogen storage alloys were investigated. XRD and BSE results indicate that $LaNi_{3.55}Co_{0.2}Mn_{0.35}Al_{0.15}Cu_{0.75}$ alloy is single $LaNi_5$ phase, and the alloys containing $V_{0.81}Fe_{0.19}$ consist of $LaNi_5$ phase, Ni-rich second phase and La-rich segregation, and the abundant of secondary phase increases with increasing x value. The activation property of alloy electrodes is improved by increasing $V_{0.81}Fe_{0.19}$ content. The C_{max} of the alloy electrodes first increases from 325.9 mAh/g (x = 0) to 330.3 mAh/g (x = 0.05), and then decreases to 301.3 mAh/g (x = 0.20). HRD_{1200} first increases from 43.3% (x = 0) to 58.5% (x = 0.05), and then decreases to 47.4% (x = 0.20), which is

related to the charge-transfer reaction on the interface and hydrogen diffusion in bulky alloy. Cycling stability decreases with increasing *x* from 0 to 0.20.The adequate substitution of Co by VFe can improve the electrochemical performances and reduce the raw cost of alloy electrode.

ACKNOWLEDGEMENTS
This research is financially supported by the National Natural Science Foundation of China (51001043), Program for New Century Excellent Talents in University, China Postdoctoral Science Special Foundation (201104390), China Postdoctoral Science Foundation (20100470990), Program for Innovative Research Team (in Science and Technology) in the University of Henan Province (No. 2012IRTSTHN007), Baotou Science and Technology Project (2011J1003) and the Doctoral Foundation of Henan Polytechnic University (B2010-13).

References

1. B. Liao, Y.Q. Lei, L.X. Chen, G.L. Lu, H.G. Pan and Q.D. Wang, *J. Alloys Compd.*, 376 (2004) 186
2. S. Bliznakov, E. Lefterova, N. Dimitrov, K. Petrov and A. Popov, *J. Power Sources*, 176 (2008) 381
3. W.K. Hu, D.M. Kim, K.J. Jang and J.Y. Lee, *J. Alloys Compd.*, 269 (1998) 254
4. C. Khaldi, H. Mathlouthi, J. Lamloumi and A. Percheron-Guégan, *Int. J. Hydrogen Energy*, 29 (2004) 307
5. W.K. Hu. *J. Alloys Compd.*, 289 (1999) 299
6. S. Yang, Y. Li, Z. Liu, S. Yang and S. Han, *Acta Phys.-Chim. Sin.*, 26 (2010) 2144
7. S. Pandey, A. Srivastava and O. Srivastava, *Int. J. Hydrogen Energy*, 32 (2007) 2461
8. M. B. Moussa, M. Abdellaoui, H. Mathlouthi, J. Lamloumi and A. Percheron Guegan, *J. Alloys Compd.*, 458 (2008) 410
9. A. Zuttel, D. Chartouni, K. Gross, P. Spatz, M. Bachler, F. Lichtenberg, A. Folzer and N.J.E. Adkins, *J. Alloys Compd.*, 253–254 (1997) 626
10. Y. Zhao, Y. Zhang, G. Wang, X. Dong, S. Guo and X. Wang, *J. Alloys Compd.*, 388 (2005) 284
11. C. Seo , S. Choi, J. Choi, C. Park and J. Lee, *Int. J. Hydrogen Energy*, 28 (2003) 967
12. C. Seo , S. Choi, J. Choi, C. Park and J. Lee, *J. Alloys Compd.*, 351 (2003) 255
13. R. Li, J.M Wu, H. Su and S.X. Zhou, *J. Alloys Compd.*, 421 (2006) 258
14. K.Y. Shu , S.K. Zhang, Y.Q. Lei, G.L. Lü and Q.D. Wang, *Int. J. Hydrogen Energy*, 28 (2003) 1101
15. Y. Zhao, Y. Zhang, G. Wang, X. Dong, S. Guo and X. Wang, *J. Alloys Compd.*, 388 (2005) 284
16. W. Choi, K. Yamataka, S. Zhang, H. Inoue and C. Iwakura, *J. Electrochem. Soc.*, 146 (1999) 46
17. C. Iwakura, W. Choi, S. Zhang and H. Inoue, *Electrochim. Acta*, 44 (1999) 1677
18. D. Yan, G. Sandrock and S. Suda, *J. Alloys Compd.*, 216 (1994) 237
19. R. Brateng, S. Gulbrandsen-Dahl, L.O. Vaøen, J.K. Solberg and R. Tunold, *J. Alloys Compd.*, 396 (2005) 100
20. S.R. Ovshinsky, M.A. Fetcenko and J. Ross, *Science*, 260 (1993) 176
21. X.B. Zhang, D.Z. Sun, W.Y. Yin, Y.J. Chai and M.S. Zhao, *Chem Phys Chem*, 6 (2005) 520
22. H.G. Pan, J.X. Ma, C.S. Wang, S.A. Chen, X.H. Wang and Q.D. Wang, *J. Alloys Compd.*, 293-295 (1999) 648
23. P. Notten and P. Hokkeling, *J. Electrochem. Soc.*, 138 (1991) 1877
24. G. Zheng, B.N. Popov and R.E. White, *J. Electrochem. Soc.*, 142 (1995) 2695
25. B. Liu, G. Fan, Y. Wang, G. Mi, Y. Wu and L. Wang, *Int. J. Hydrogen Energy*, 33 (2008) 5801
26. C. Khaldi, H. Mathlouthi, J. Lamloumi and A. Percheron-Guegan, *J. Alloys Comp.*, 360 (2003) 266

27. C. Iwakura, M. Miyamoto, H. Inoue, M. Matsuoka and Y. Fukumoto. *J. Alloys Compd.*, 259 (1997), pp.
28. T. Sakai, K. Oguro, H. Miyamura, N. Kuriyama, A. Kato and H. Ishikawa, *J. Less-Com. Met.*, 161(1990) 193
29. D. Chartouni, F. Meli, A. Zuttel, K. Gross and L. Schlapbach, *J. Alloys Compd.*, 241 (1996) 160
30. Q. Lin, S. Zhao, D. Zhu, B. Song and Z. Mei, *J. Alloys Compd.*, 351 (2003) 91
31. M. Fetcenko, S. Venkatesan and S. Ovshinsky, in: Proceedings of the Symposium on Hydrogen Storage Materials, Batteries and Electrochemistry, The Electrochemical Society, 1992, 141.

© 2012 by ESG (www.electrochemsci.org)